LASER INTERFEROMETER GRAVITATIONAL WAVE OBSERVATORY
- LIGO -
CALIFORNIA INSTITUTE OF TECHNOLOGY
MASSACHUSETTS INSTITUTE OF TECHNOLOGY

Technical Note	**LIGO-T070193-00-I**	October 26, 2007

Next-generation Radio Frequency Photodiodes for Gravitational-Wave Interferometers

Alice Z. Wang
Mentors: Rana Adhikari and Alan Weinstein

Distribution of this document:
LIGO Scientific Collaboration

California Institute of Technology
LIGO Project, MS 18-34
Pasadena, CA 91125
Phone (626) 395-2129
Fax (626) 304-9834
E-mail: info@ligo.caltech.edu

Massachusetts Institute of Technology
LIGO Project, Room NW17-161
Cambridge, MA 02139
Phone (617) 253-4824
Fax (617) 253-7014
E-mail: info@ligo.mit.edu

LIGO Hanford Observatory
Route 10, Mile Marker 2
Richland, WA 99352
Phone (509) 372-8106
Fax (509) 372-8137
E-mail: info@ligo.caltech.edu

LIGO Livingston Observatory
19100 LIGO Lane
Livingston, LA 70754
Phone (225) 686-3100
Fax (225) 686-7189
E-mail: info@ligo.caltech.edu

1   Abstract

The Laser Interferometer Gravitational-wave Observatory (LIGO) detects gravitational waves by sensing minute relative displacements of test mass mirrors using the interference formed by laser beams which are modulated at radio frequencies. The light beams are detected by multiple radio frequency photodiodes monitoring the displacements and angular motion of the interferometer. This project entails the design, development, and testing of a new radio frequency photodiode preamplifier for improved performance. Instead of a resonant circuit around the photodiode and a single tank filter for the unwanted first harmonic signal as in the circuit currently used in the interferometers, the new design uses parallel capacitor-inductor tank circuits to increase diode capacitance insensitivity, decrease signal nonlinearity, and optimize signal isolation. Test results from a prototype circuit as well as circuit analysis models show improvements made on the radio frequency photodiodes. Data gathered from this project also provide useful component specifications for future photodiode development.

2   Introduction

Gravity as radiation waveforms was first predicted by Einstein in his General Relativity and was confirmed as a material reality with evident energy loss from the Hulse-Taylor binary. The Laser Interferometer Gravitational Wave Observatory (LIGO) seeks to detect gravitational waves by using two Michelson Interferometers, one with 4km arms and the other with 2km arms, in Washington and another 4km-arm Michelson interferometer in Louisiana[1]. When a gravitational wave passes by, it stretches one arm of the interferometer while contracting the other arm, causing a displacement to be measured by LIGO through the change in the interference of the laser beams in the interferometer. The detection of gravitational waves would confirm present knowledge of general relativity as well as open up a new science of gravitational wave astronomy[2].

Initial LIGO took its first scientific data in 2002 and had four science runs since then. Design sensitivities were finally reached in November of 2005, and Initial LIGO is currently on its fifth and last science run. After the fifth science run, installation of Enhanced LIGO will begin, and Advanced LIGO (AdvLIGO) a few years after that. The much anticipated AdvLIGO will be about ten times more sensitive and able to listen to a volume of space a thousand times greater than Initial LIGO[3].

The Caltech LIGO 40-meter lab houses a prototype interferometer with 40 meter long arms and acts as a testing ground for new technologies to be implemented in Enhanced and Advanced LIGO. Although the 40-meter interferometer does not expect to detect gravitational waves, working on and improving the prototype interferometer provides many ideas and results for the full-sized interferometers at Hanford and Livingston.
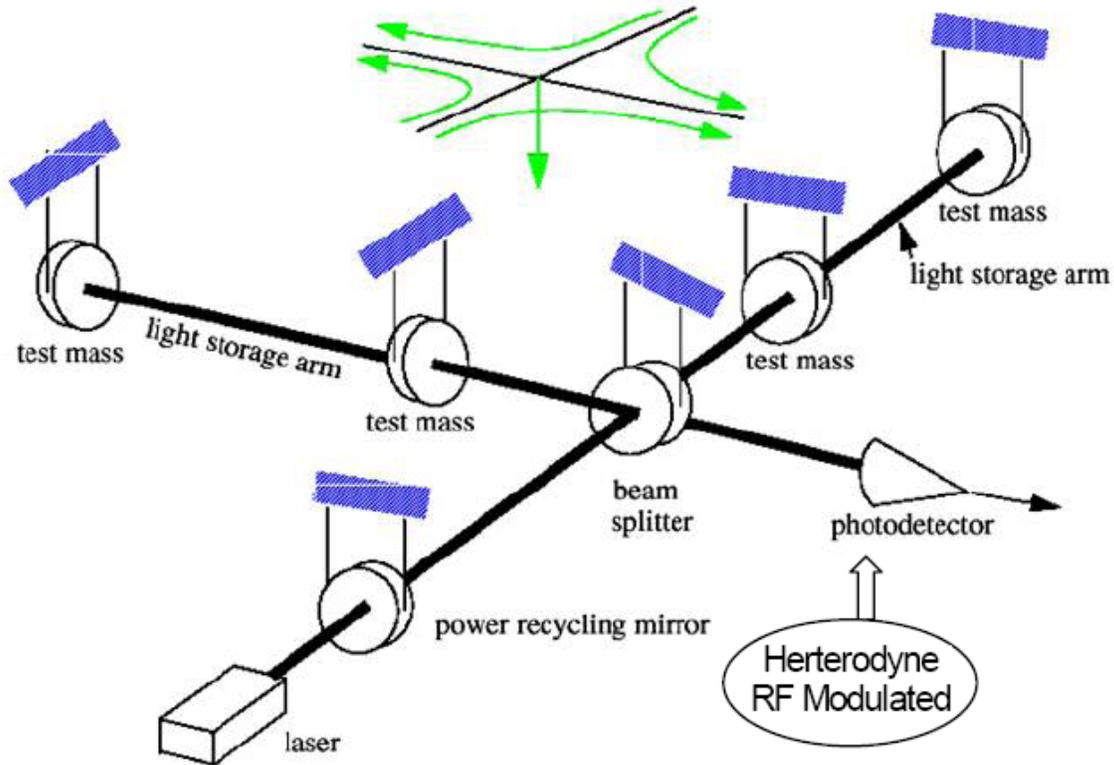
Figure 1: A Michelson interferometer as those used in LIGO. A gravitational wave would stretch one arm of the L-shaped configuration while contracting the other, thus producing a minute change in the lengths of the cavities and thus a change in the interference pattern of the laser beam on the photodetector[2]. Only one of the many RF photodetectors used to sense the mirror positions is shown in figure.

3   Background

3.1   Photodetectors in LIGO

LIGO uses many photodetectors in multiple locations in the interferometers to monitor the displacements and angular motion for multiple degrees of freedom. The most demanding use for photodetectors in the interferometer has been in the dark port to detect gravitational wave signal in the laser beam interference. Because the interferometer uses a heterodyne readout technique where the laser beam is modulated at radio frequencies so that the beam at the dark port carries the information in the amplitude of a beat signal of two frequencies. Figure 1 shows the layout of a Michelson interferometer like those used in Initial LIGO.

In AdvLIGO, RF photodetectors will continue to be used in at least a dozen locations within the AdvLIGO interferometers. Gravitational wave detectors have special requirements for their photodetectors. Since higher laser power increases the sensitivity of the detectors, the LIGO photodetectors need to detect as high of a laser power as possible and detect a large signal size with
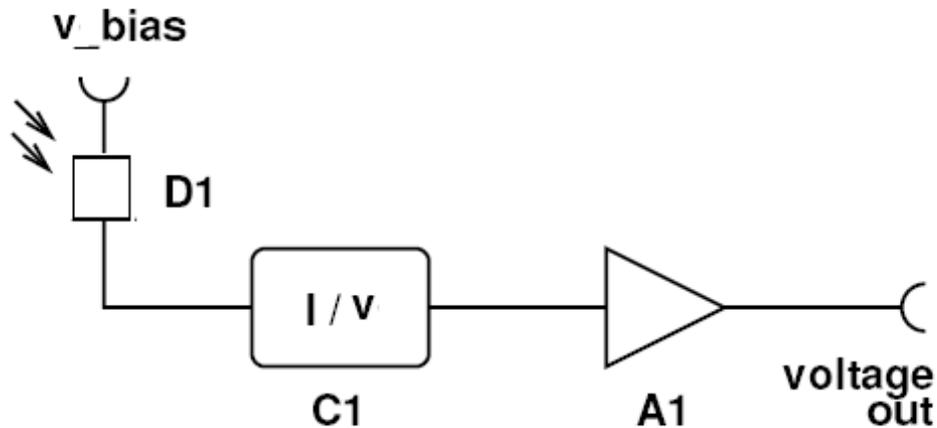
Figure 2: Basic principle of a photodetector circuit. V_Bias is the bias voltage applied, D1 is the photodiode, C1 is the preamplifier circuit, and A1 is the voltage amplifier[4].

a noise floor dominated by photon shot-noise at the radio frequency detection frequencies. Also, other signals from the different detection frequencies should not disturb the measurement of the desired detection frequency signal.

4 Photodetector Circuit

Figure 2 shows the basic working principle of a photodetector circuit. A bias voltage is applied to the photodiode (D1), which generates a current as the light hits it. As such, the diode can be seen approximately as a current generator. The preamplifier circuit acts as a current-to-voltage converter with a conversion factor of transimpedance $Z = V/I$. The signal is then sent to an operational amplifier for amplification and output[4].

More precisely, the photodiode is modeled as a current generator with inherent resistance and capacitance, shown in Figure 3. This is the model used in the circuit analysis in this project.

5 Initial LIGO Photodetector

Figure 4 shows the photodetector circuit used in Initial LIGO. The circuitry shown above the diode (D1) itself provides the bias voltage for the photodiode. A resonant circuit is formed by the inherent capacitance of the diode and L1, tuned to the detection frequency. The tank circuit formed by C2 and L2 forms a notch filter which filters out the unwanted first harmonic signal. The signal then
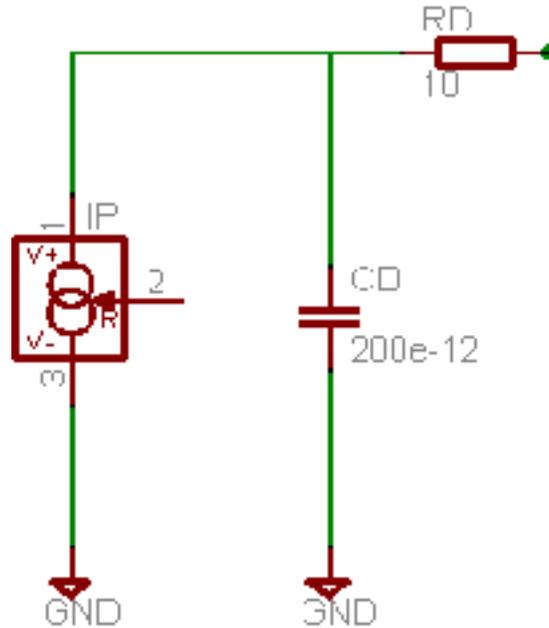
Figure 3: The diode model used. IP is the input photocurrent, CD is the diode capacitance, and RD is the diode resistance.
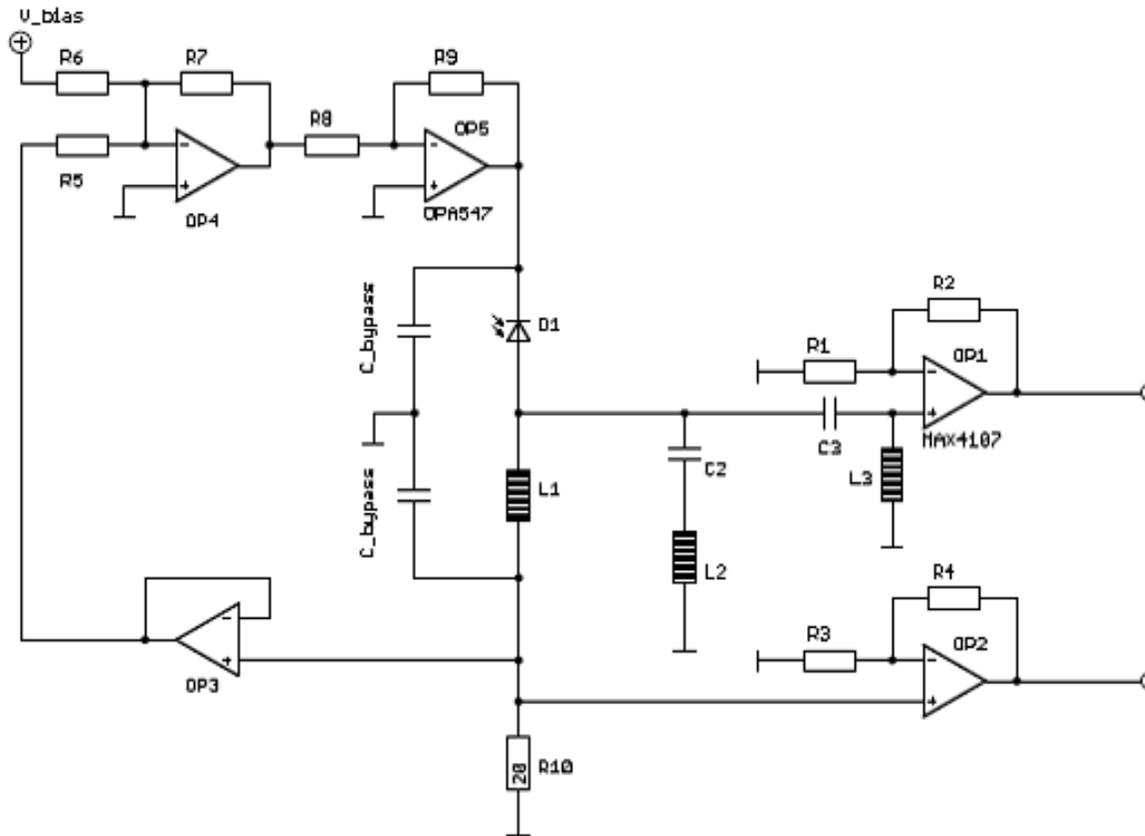

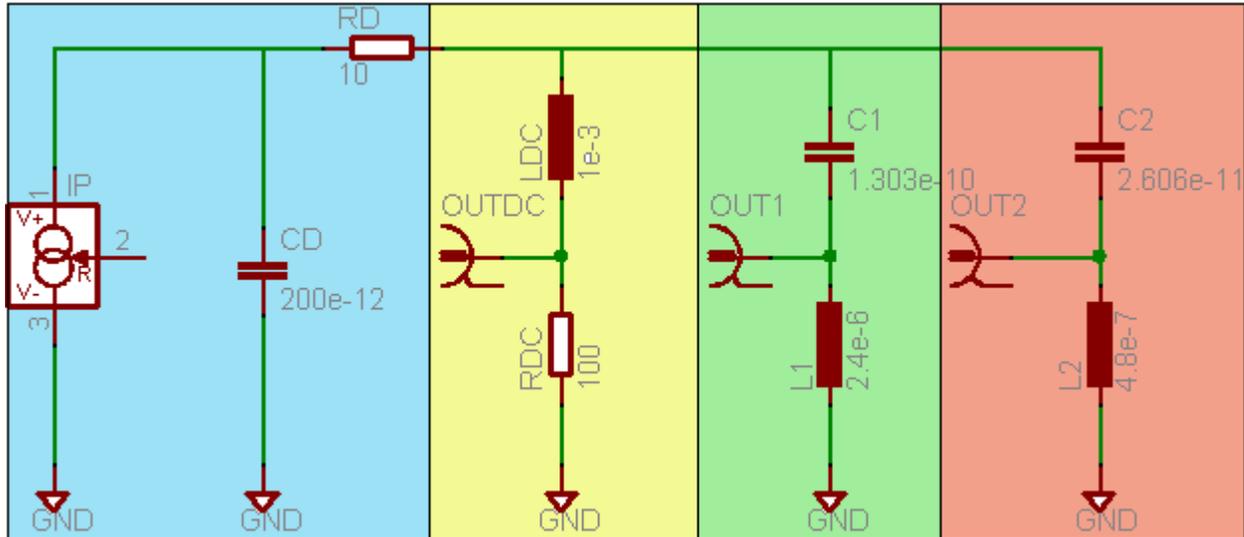Figure 4: The photodetector circuit currently used in Initial LIGO[4].

Figure 5: Circuit diagram of new photodetector preamplifier design. The blue section of the circuit contains the model of the the diode, the yellow section the DC output, the green and orange sections capacitor-inductor tank circuit branches tuned to detection frequencies.

passes through a high pass filter formed by C3 and L3 before reaching the operational amplifier OP1 for output.

This circuit topology poses several disadvantages, the most important of which is the fact that the signal voltage appears across the photodiode, which is very undesireable for large signal sizes. Because the capacitance of the photodiode itself is used to create the resonance in the signal, the signal voltage appears across the diode, modulating the bias voltage of the photodiode, causing non-linearities in the signal which leads to additional noise and shifts in resonance frequency. Also, the signal is very sensitive to the choice of photodiode since the resonant circuit includes the diode capacitance. Ideally, the preamplifier circuit should be as independent from the the diode as possible in case the photodiode needs to be replaced.

6   New Photodetector Design

Figure 5 shows a circuit diagram of the new design of photodetector circuit using the concepts of the current photodetector circuit used at the GEO 600 gravitational wave detector. The first CL tank circuit is tuned to resonate at a detection frequency of 9MHz, and the second CL tank circuit is tuned to resonate at a detection frequency of 45MHz. Instead of having the signal appear full-strength at the photodiode anode, the photocurrent flows into a series CL resonant circuit at detection frequency and outputs at the nodes between the capacitors and inductors. Thus, the two tank circuits act as notch filters at the diode anode at detection frequencies. Also, since the two tank circuits are parallel to each other, the 9MHz tank branch acts as a notch for the 9MHz signal at 45MHz and vice versa, maximizing the ratios of the desired detection frequecy over the other. The final circuit design will include four parallel tank circuits with the additional two branches
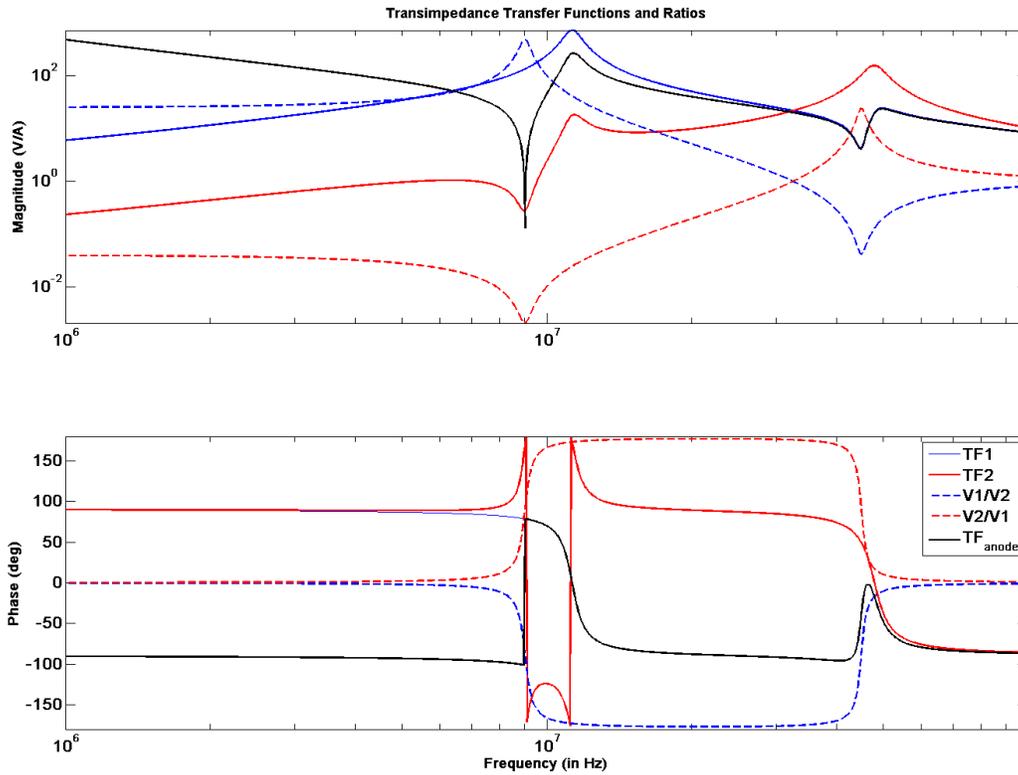
Figure 6: Transimpedance transfer functions and ratios of the new photodetector circuit. TF1 and TF2 are the transfer functions from the current I_{IP} at the photodiode to the voltages at OUT1 and OUT2, respectively, with units of V/A. TF_{anode} is the transfer function seen by the anode of the photodiode, from I_{IP} to the anode of the diode at the node between RD and the tank branches in Fig. 5. $V1/V2$ and $V2/V1$ are the ratios of the detection frequency signals where V1 is the 9MHz signal voltage out of OUT1 and V2 is the 45MHz signal voltage out of OUT2.

tuned to the beat frequencies of 9MHz and 45 MHz. For the purposes of this analysis, however, only the 9MHz and 45MHz branches are considered as a simpler model.

As can be seen in Figure 6, the impedance seen by the photodiode anode at the detection frequencies are much lower than the transimpedance for the total current-to-voltage conversion of the circuit since the two CL tank circuits form notches in the TF_{anode} transfer function at the detection frequencies. This prevents the signal voltage from appearing across the photodiode and modulating the bias voltage and the subsequent non-linearities. Each of the tank circuit transfer functions forms a notch at the detection frequency of the other, causing a peak in its ratio over the other at its own detection frequency. This shows the great isolation of the desired detection frequency signal from the total signal achieved by this new design. Since the resonance frequency of the detection frequency signals is no longer produced by the diode capacitance, the preamplifier is almost entirely insensitive to the differences in the photodiode. Notice that the transfer functions of the tank circuits do not peak at their detection frequencies of 9MHz and 45MHz, respectively. Instead, a resonance peak occurs in both transfer functions at 11MHz and another occurs at 48MHz. These
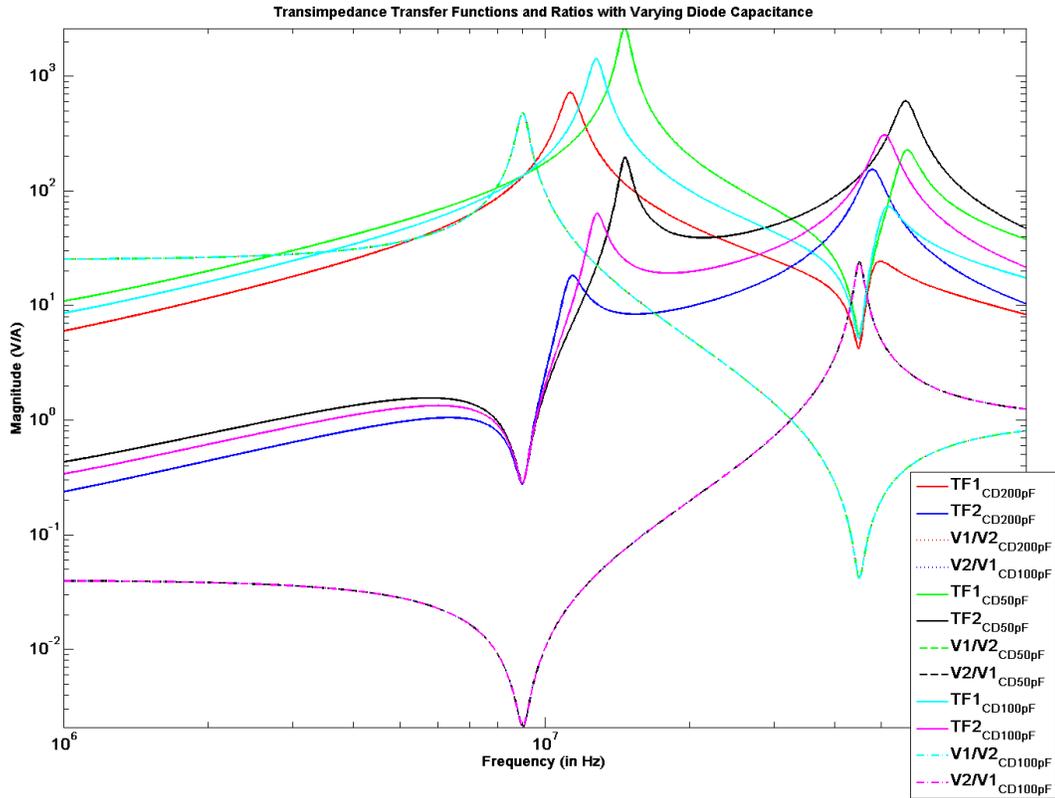
Figure 7: Transfer functions of the two tank circuits with varied diode capacitances.

resonant peaks are caused by parasitic resonances of the inductors and capacitors of the parallel branches of the circuit and not very important in considering this circuit. When the capacitance of the photodiode is changed, the rest of the transfer function curves are changed, but the point at the detection frequency of the tank circuit stays almost constant, as shown in Figure 7. This makes the point on the tank circuit transfer functions at its detection frequency not only the point at which is the desired signal voltage peaks over other signals present, but also the most diode capacitance insensitive on the transfer function. Also, the ratio functions are not changed at all by the varied diode capacitance (the ratios of each varied capacitance case lay on top of each other).

7   Signal-to-Noise Ratio Analysis

A gravitational wave detector photodetector needs to be shot-noised limited with a noise floor dominated by the photon shot noise, which means the shot noise must be greater than other noise sources by several factors. Photon shot noise is a quantum fluctuation in the photocurrent caused by the discrete nature of photons. To show the dominance of shot noise over electronic noise sources in the circuit, a signal-to-noise ratio analysis was performed with shot noise, I_{shot} as the signal[5]. I_{shot} is a current noise spectral density in units of $\frac{A}{\sqrt{Hz}}$. Shot noise is a white noise, and I_{IP}

Photodiode and Circuit Parameters

Parameter	Symbol	Value	Units
Input referred voltage noise of op-amp	V_n	2	nV/√Hz
Input referred current noise of op-amp	I_n	3	pA/√Hz
DC Photocurrent	IP	50	mA
Diode Capacitance	CD	200	pF
Diode Resistance	RD	10	Ω
DC Trap Inductance	LDC	1	mH
DC Trap Resistance	RDC	100	Ω
9MHz Trap Capacitance	C1	0.13	nF
9MHz Trap Inductance	L1	2.4	μH
9MHz Trap Inductor Resistance	R_{L1}	5.43	Ω
45MHz Trap Capacitance	C2	0.026	nF
45MHz Trap Inductance	L2	0.48	μH
45MHz Trap Inductor Resistance	R_{L2}	6.8	Ω

Figure 8: Table of parameters used in SNR analysis.

is the DC photocurrent:

$$I_{shot} = \sqrt{2eI_{IP}} \tag{1}$$

7.1 Signal Calculation

The signal voltages at OUT1 and OUT2 are determined by the current through the branch of the tank circuit, calculated by Kirchhoff's Laws, multiplied by the impedance of the tank inductor, according to generalized Ohm's Law:

$$V_{out} = I_{tank}(i\omega L_{tank} + R_L) \tag{2}$$

where I_{tank} is the current through any of the branches of tank circuits, ω is $2\pi \times f$ of the signal, L_{tank} is the inductance of the tank inductor, and R_L is the resistance of the tank inductor.

As can be seen in Figure 9, the signal sizes at OUT1 and OUT2 are almost the same since the transimpedances of the two tanks are tuned to be as equal as possible. The signal at OUT1 is about $1.69 \times 10^{-8}V$, and the signal at OUT2 is about $1.28 \times 10^{-8}V$.

7.2 Noise Calculation

The noise sources taken into account in this SNR calculation were the input voltage and current noise of the operational amplifier used (as shown in figure 8) and the Johnson thermal noise of the
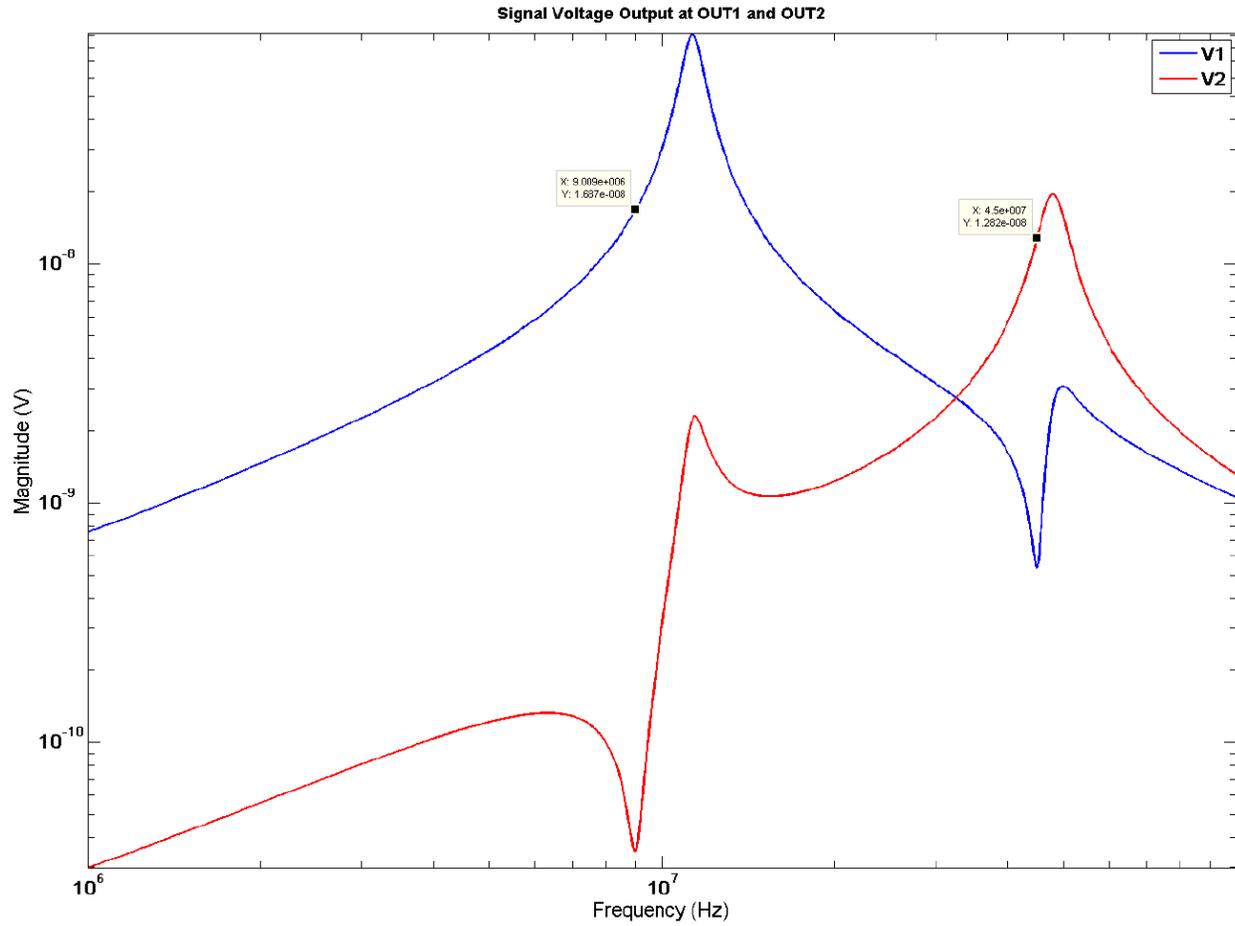
Figure 9: Plot of signal voltage out of each detection frequency output. V1 is the voltage out of OUT1 while V2 is the voltage out of OUT2.

circuit. The amount of electronic noise in $\frac{V}{\sqrt{Hz}}$ is calculated by:

$$N = \sqrt{V_n^2 + (I_n Z_{system})^2 + V_J^2}$$ (3)

where V_n is the input referred voltage noise of the operational amplifier, I_n is the input referred current noise of the operational amplifier, Z_{system} is the impedance of the system as seen by the non-inverting input of the operational amplifier, and V_J is the Johnson noise, as given by:

$$V_J = \sqrt{4K_B T Re(Z_{system})}$$ (4)

where K_B is Boltzmann's Constant and T is the temperature in Kelvins, assumed to be $300K$.

According to these calculations, the noise at OUT1 at 9MHz is $2.03 \times 10^{-9} \frac{V}{\sqrt{Hz}}$, and the noise at OUT2 at 45MHz is $2.05 \times 10^{-9} \frac{V}{\sqrt{Hz}}$. Thus, the SNR at OUT1 at 9MHz is 7.2, and the SNR at OUT2 at 45MHz is 6.2, both an improvement on Initial LIGO's photodetector SNR of 6.1.

Output	Signal (V)	Noise $(\frac{V}{\sqrt{Hz}})$	SNR
OUT1	1.69×10^{-8}	2.03×10^{-9}	7.2
OUT2	1.28×10^{-8}	2.05×10^{-9}	6.2

The above table summarizes the results of the SNR analysis.

8   Wave-Front Sensor Photodetectors

Measurements of the transfer functions of the LIGO wavefront sensor photodiodes were taken to assess the quality of the current photodiodes. An HP4195A network analyzer outputted a spectrum sweep to an RFAM test laser which was shined on a quadrant of a photodiode, the output of which was connected to the network analyzer recording the transfer functions of that quadrant. The HP4195A network analyzer had no accessible built-in data acquisition interface, so a MATLAB function was written to easily import data from the network analyzer to a computer via a GPIB cable. The function is included in the appendix of this document. Since the responses of the quadrants on a photodiode is supposed to match each other, the transfer functions of the four quadrants of each photodiode were plotted on one graph for comparison. For a more valid comparison, the measurement DC voltages are first divided from each transfer function. Figure 10 shows the results from photodiode 1 of the wave-front sensors, and Figure 11 shows the results from photodiode 2.

The wavefront sensor photodiodes are supposed to have resonance peaks at around 29MHz and notches at the first harmonic frequency. As can be seen from the plots, the wave-front sensor photodiodes are not tuned very well since the peaks and notches of each quadrant are not very close to each other.
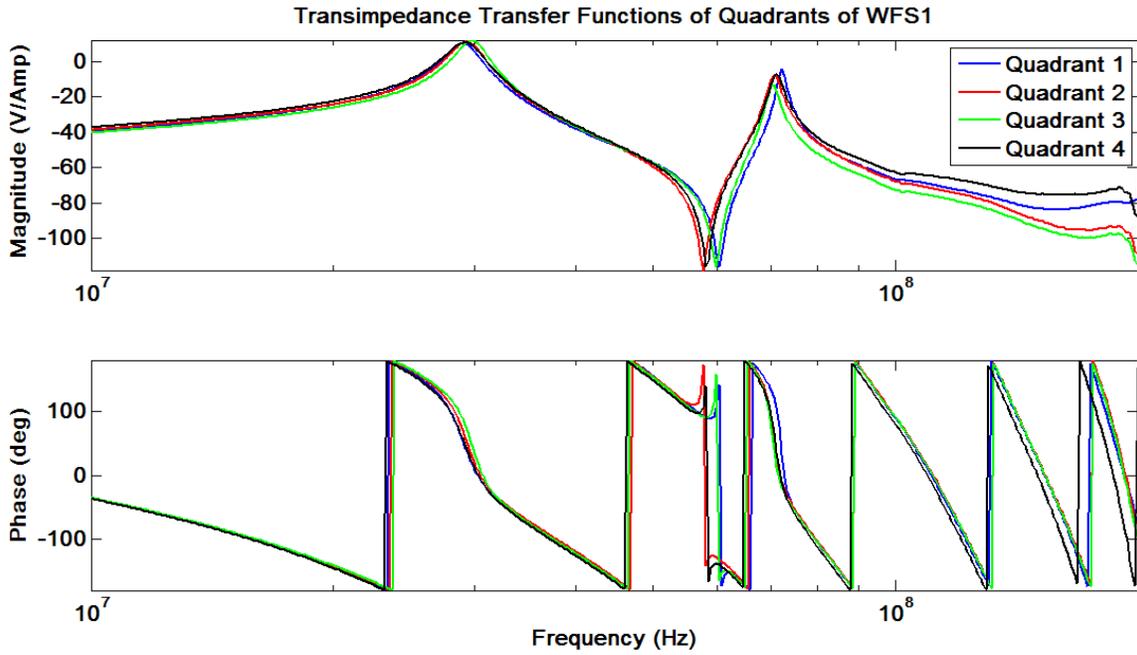
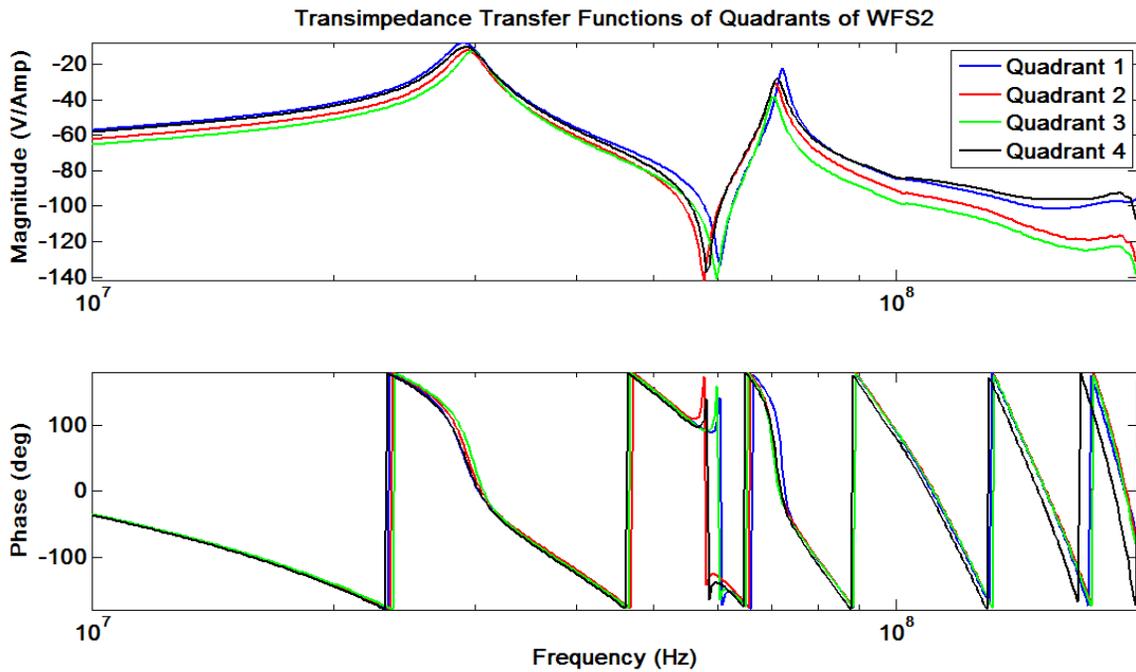Figure 10: Plot of the transfer functions of the quadrants of wave-front sensor photodiode 1.

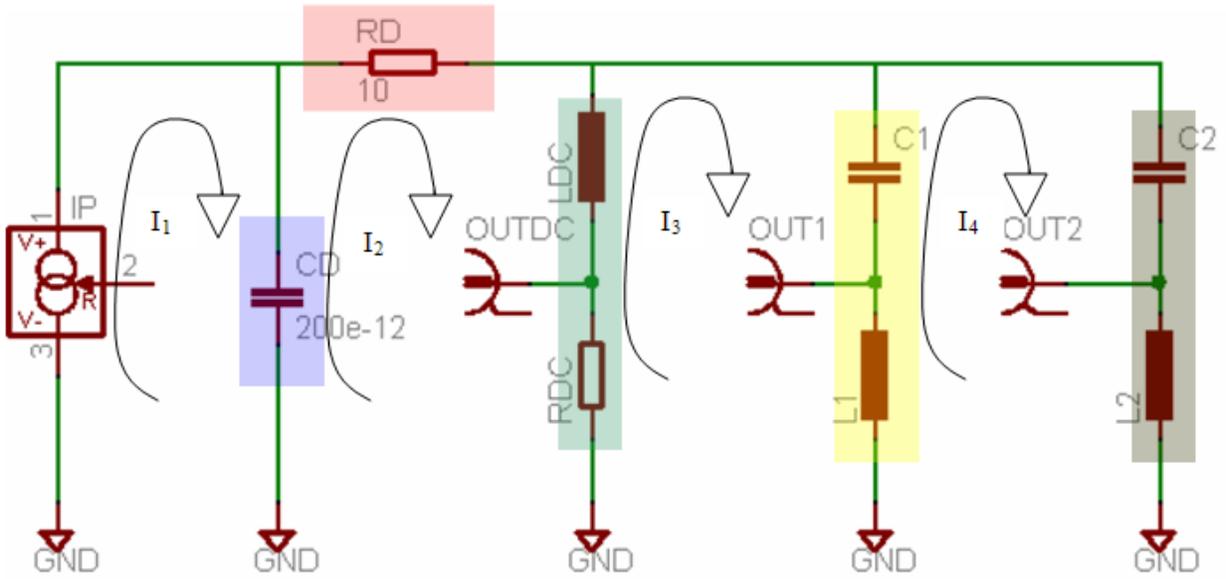Figure 11: Plot of the transfer functions of the quadrants of wave-front sensor photodiode 2.

Figure 12: Circuit diagram with the currents used in the mesh analysis labeled. The colored boxes denote the impedances grouped together in the analysis for convenience.

9   Methods

The analysis presented in this paper was performed with mesh analysis on the parallel LC branch circuit as shown in Figure 12.

In subsequent calculations, the impedance of the capacitor in the blue box will be known as Z_2, the impedance of the resistor in the pink box will be known as Z_1, the total impedance of the elements in the green box will be known as Z_3, the total impedance of the elements in the yellow box will be known as Z_6, and the total impedance of the elements in the gray box will be known as Z_5.

I_1 is equal to the input current from the photodiode, I_{shot}, in the first mesh loop. The equations written for the other three loops are:

$$Z_1 I_2 + Z_3(I_2 - I_3) + Z_2(I_2 - I_1) = 0 \tag{5}$$

$$Z_6(I_3 - I_4) + Z_3(I_3 - I_2) = 0 \tag{6}$$

$$Z_6(I_4 - I_3) + Z_5 I_4 = 0 \tag{7}$$

To solve for the voltages at OUT1 and OUT2, the value of I_4 is needed. A matrix equation formed from the mesh equations can be used to solve for the mesh currents:

$$\begin{pmatrix} (\text{-}Z_2) & (Z_1 + Z_2 + Z_3) & (\text{-}Z_3) & 0 \\ 1 & 0 & 0 & 0 \\ 0 & (\text{-}Z_3) & (Z_3 + Z_6) & (\text{-}Z_6) \\ 0 & 0 & (\text{-}Z_6) & (Z_5 + Z_6) \end{pmatrix} \begin{pmatrix} I_1 \\ I_2 \\ I_3 \\ I_4 \end{pmatrix} = \begin{pmatrix} 0 \\ I_{shot} \\ 0 \\ 0 \end{pmatrix}$$

Mathematica was used to solve the matrix equation, and the following result for I_4 were obtained:

$$I_4 = \frac{(I_{shot}Z_2Z_3Z_6)}{(Z_1Z_3Z_5 + Z_2Z_3Z_5 + Z_1Z_3Z_6 + Z_2Z_3Z_6 + Z_1Z_5Z_6 + Z_2Z_5Z_6 + Z_3Z_5Z_6)} \tag{8}$$

To calculate the signal voltage at OUT2, I_4 is multiplied by the impedance of L2:

$$V2 = i\omega L_2 \frac{(I_{shot}Z_2Z_3Z_6)}{(Z_1Z_3Z_5 + Z_2Z_3Z_5 + Z_1Z_3Z_6 + Z_2Z_3Z_6 + Z_1Z_5Z_6 + Z_2Z_5Z_6 + Z_3Z_5Z_6)} \tag{9}$$

Since Z_6 is parallel with Z_5, they can switch positions as drawn in the circuit diagram. Therefore, the I_4 calculated can also be used to produce the signal voltage at OUT1 if all the Z_6 are switched for Z_5 and vice versa and then multiplied by the impedance of L1:

$$V1 = i\omega L_1 \frac{(I_{shot}Z_2Z_3Z_5)}{(Z_1Z_3Z_5 + Z_2Z_3Z_5 + Z_1Z_3Z_6 + Z_2Z_3Z_6 + Z_1Z_5Z_6 + Z_2Z_5Z_6 + Z_3Z_5Z_6)} \tag{10}$$

To calculate the transfer functions out of each of the outputs, the signal voltage was divided by the input shot current, since the transimpedance transfer function of a photodiode circuit is defined as the output voltage over the input current:

$$TF_{output} = \frac{V_{output}}{I_{shot}} \tag{11}$$

To calculate the noise in the SNR analysis using Eq. 3, the Z_{system} needed to be calculated for each output. The Z_{system} is different for each output because the impedance is calculated with the circuit redrawn so that it is the impedance of the total system as seen by the output. Figure 13 shows the circuit diagram and Figure 14 shows the equation used to calculate the Z_{system} for the noise calculation at OUT1. Figure 15 shows the circuit diagram and Figure 16 shows the equation used to calculate the Z_{system} for the noise calculation at OUT2.

10   Acknowledgements

Figure 13: Diagram of the circuit redrawn to calculate the impedance of the system as measured from OUT1.

$$\frac{1}{Z_{System_1}} = \frac{1}{j\omega L_1 + R_{L_1}} + \frac{1}{\dfrac{1}{j\omega(C_1 + C_2)} + j\omega L_2 + R_{L_2}} + \frac{1}{\dfrac{1}{j\omega C_1} + j\omega L_{DC} + R_{DC}} + \frac{1}{R_D + \dfrac{1}{j\omega(C_1 + C_D)}}$$

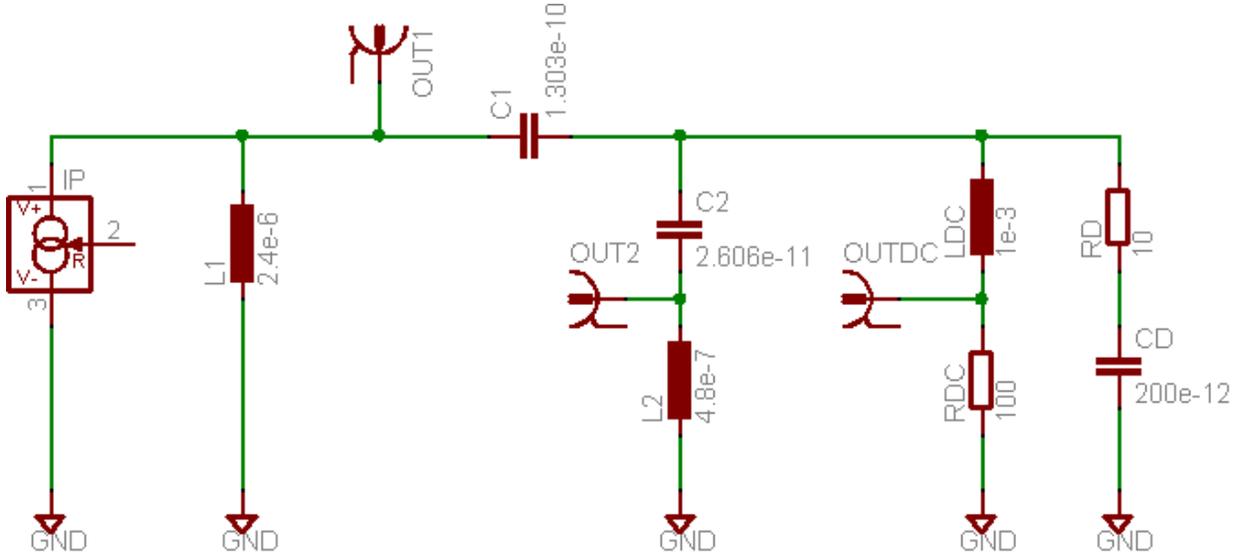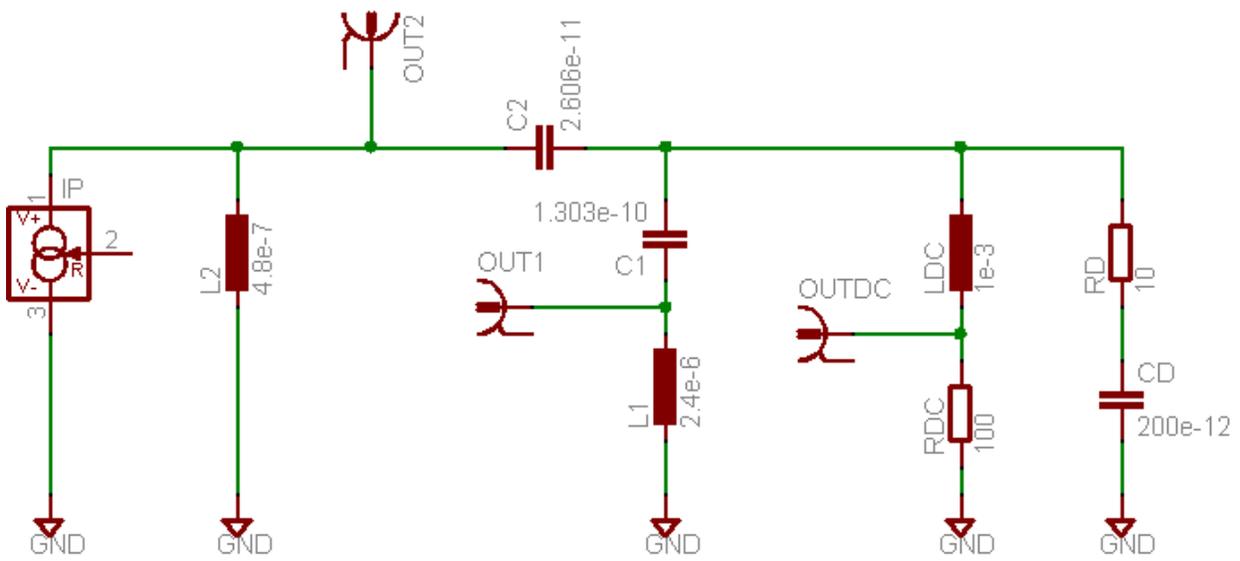Figure 14: Equation used to calculate Z_{system} at OUT1.

Figure 15: Diagram of the circuit redrawn to calculate the impedance of the system as measured from OUT2.

$$\frac{1}{Z_{System_2}} = \frac{1}{j\omega L_2 + R_{L_2}} + \frac{1}{\dfrac{1}{j\omega(C_1 + C_2)} + j\omega L_1 + R_{L_1}} + \frac{1}{\dfrac{1}{j\omega C_2} + j\omega L_{DC} + R_{DC}} + \frac{1}{R_D + \dfrac{1}{j\omega(C_2 + C_D)}}$$

Figure 16: Equation used to calculate Z_{system} at OUT2.

11   References

[1]Weinstein, Alan. SURF Lectures. 2007 <http://www.ligo.caltech.edu/ ajw/ligo_SURF_060616.pdf>

[2]Christensen, Nelson. "Searching for Gravitational Waves" LIGO Scientific Collaboration. 2006 <http://www.ligo.caltech.edu/ ajw/IntroPapers/christensen.pdf>

[3]Cadonati "Listening to Space with LIGO" 2006 <http://www.ligo.caltech.edu/ ajw/IntroPapers/cadonati_06.pdf>

[4]Grote, Harmut. "High-Power, Low-Noise, and Multiple Resonant Photodetector for Interferometric Gravitational wave Detectors." Max-Planck-Institut fur Gravitationsphysik (Albert-Einstein-Institut) und Universitat Hannover, Callinstr. 38, D-30167 Hannover <http://www.ligo.caltech.edu/ rana/docs/Hartmut-RFPDs.pdf>

[5]Abbott, Rich. "RFPD Topology Comparison." LIGO-T060268-01-C. Nov. 6, 2006

12   Appendix: MATLAB Code

```
clear
clc
close all

set(0,'DefaultLineLineWidth',1.5);
set(0,'DefaultAxesFontSize',16);
set(0,'DefaultAxesFontWeight','demi');
Is=sqrt(2*1.602e-19*50e-3);
rd=10;
cd=200e-12;
ldc=1e-3;
rdc=100;
rl1=0.5*5;
c1=0.2*5.8e-10;
l1=538*5e-9;
l2=111*5e-9;
rl2=0.3*5;
c2=0.2*1.1e-10;
Kb=1.38e-23;
T=300;
vn=2e-9;
in=3e-12;
w=2*pi*logspace(6,8.01,1000);

x=j.*w;
Z1=rd;
Z2=1./(x.*cd);
Z3=x.*ldc+rdc;
Z6=1./(x.*c2)+x.*l2+rl2;
Z5=1./(x.*c1)+x.*l1+rl1;

I1=Is;
I2=(Is.*Z2.*Z3.*Z5 + Is.*Z2.*Z3.*Z6 + Is.*Z2.*Z5.*Z6)./(Z1.*Z3.*Z5 +...
    Z2.*Z3.*Z5 + Z1.*Z3.*Z6 + Z2.*Z3.*Z6 + Z1.*Z5.*Z6 + Z2.*Z5.*Z6 +...
    Z3.*Z5.*Z6);
I3=(Is.*Z2.*Z3.*(Z5 + Z6))./(Z1.*Z3.*Z5 + Z2.*Z3.*Z5 + Z1.*Z3.*Z6 +...
    Z2.*Z3.*Z6 + Z1.*Z5.*Z6 + Z2.*Z5.*Z6 + Z3.*Z5.*Z6);
I4=(Is.*Z2.*Z3.*Z6)./(Z1.*Z3.*Z5 + Z2.*Z3.*Z5 + Z1.*Z3.*Z6 +
Z2.*Z3.*Z6...
    + Z1.*Z5.*Z6 + Z2.*Z5.*Z6 + Z3.*Z5.*Z6);
I4a=(Is.*Z2.*Z3.*Z5)./(Z1.*Z3.*Z5 + Z2.*Z3.*Z5 + Z1.*Z3.*Z6 +
Z2.*Z3.*Z6...
    + Z1.*Z5.*Z6 + Z2.*Z5.*Z6 + Z3.*Z5.*Z6);
Iv1=I4a;
Iv2=I4;
V1=Iv1.*x.*l1;
V2=Iv2.*x.*l2;
Vanode=I2./(1./Z3+1./Z5+1./Z6);
tf1=V1./Is;
tf2=V2./Is;
tfAnode=Vanode./Is;
V1rat=tf1./tf2;
V2rat=tf2./tf1;

f=w./(2*pi);
```

page 16

```matlab
figure
loglog(f,abs(V1),'b',f,abs(V2),'r')
axis tight
title('Signal Voltage Output at OUT1 and OUT2')
ylabel('Magnitude (V)')
xlabel('Frequency (Hz)')
legend('V1','V2')

figure
loglog(f,abs(tf1),'b',f,abs(tf2),'r',f,abs(tf1./tf2),'b--',f,...
    abs(tf2./tf1),'r--',f,abs(tfAnode),'k');
axis tight
title('Transimpedance Transfer Functions and Ratios');
ylabel('Magnitude (V/A)')
legend('TF1','TF2','V1/V2','V2/V1','TF_{anode}');
xlabel('Frequency (in Hz)')

figure
loglog(f,abs(tf1),'r-',f,abs(tf2),'b-
',f,abs(V1rat),'r:',f,abs(V2rat),...
    'b:','LineWidth',1.5);
hold on
cd=50e-12;
Z2=1./(x.*cd);
I4=(Is.*Z2.*Z3.*Z6)./(Z1.*Z3.*Z5 + Z2.*Z3.*Z5 + Z1.*Z3.*Z6 +
Z2.*Z3.*Z6...
    + Z1.*Z5.*Z6 + Z2.*Z5.*Z6 + Z3.*Z5.*Z6);
I4a=(Is.*Z2.*Z3.*Z5)./(Z1.*Z3.*Z5 + Z2.*Z3.*Z5 + Z1.*Z3.*Z6 +
Z2.*Z3.*Z6...
    + Z1.*Z5.*Z6 + Z2.*Z5.*Z6 + Z3.*Z5.*Z6);
Iv1=I4a;
Iv2=I4;
V1=Iv1.*x.*l1;
V2=Iv2.*x.*l2;
tf1a=V1./Is;
tf2a=V2./Is;
loglog(f,abs(tf1a),'g-',f,abs(tf2a),'k-',f,abs(tf1a./tf2a),'g--',f,...
    abs(tf2a./tf1a),'k--','LineWidth',1.5);
cd=100e-12;
Z2=1./(x.*cd);
I4=(Is.*Z2.*Z3.*Z6)./(Z1.*Z3.*Z5 + Z2.*Z3.*Z5 + Z1.*Z3.*Z6 +
Z2.*Z3.*Z6...
    + Z1.*Z5.*Z6 + Z2.*Z5.*Z6 + Z3.*Z5.*Z6);
I4a=(Is.*Z2.*Z3.*Z5)./(Z1.*Z3.*Z5 + Z2.*Z3.*Z5 + Z1.*Z3.*Z6 +
Z2.*Z3.*Z6...
    + Z1.*Z5.*Z6 + Z2.*Z5.*Z6 + Z3.*Z5.*Z6);
Iv1=I4a;
Iv2=I4;
V1=Iv1.*x.*l1;
V2=Iv2.*x.*l2;
tf1b=V1./Is;
tf2b=V2./Is;
loglog(f,abs(tf1b),'c-',f,abs(tf2b),'m-',f,abs(tf1b./tf2b),'c-.',f,...
    abs(tf2b./tf1b),'m-.','LineWidth',1.5);
axis tight




title('Transimpedance Transfer Functions and Ratios with Varying Diode
Capacitance');
legend('TF1_{CD200pF}','TF2_{CD200pF}','V1/V2_{CD200pF}',...
    'V2/V1_{CD100pF}','TF1_{CD50pF}','TF2_{CD50pF}','V1/V2_{CD50pF}',...

'V2/V1_{CD50pF}','TF1_{CD100pF}','TF2_{CD100pF}','V1/V2_{CD100pF}',...
    'V2/V1_{CD100pF}')
ylabel('Magnitude (V/A)')
xlabel('Frequency (in Hz)')
```

Figure 17: MATLAB code for the transimpedance transfer functions, output signal voltages, and transfer functions with varying diode capacitances.

```
function [data,info] = getgpibdata_HP4195A(g,info)

a = input('Is this a spectrum analysis on the HP4195A? (1=yes, 0=no):
');


fprintf(g,'FMT1')        %set output magnitude data format = 64 bit ASCII
fprintf(g,'DEG')         %set output phase data to degrees instead of
radians
fprintf(g,'DPA1')        %set trace A ON

%download data, units and bandwidth
%info.name=[info.idn, ' Data'];
data{1} = str2num(query(g,'X?'));
data{1}=data{1}(1:end)';
info.bw = str2num(query(g,'RBW?'));

if a
    fprintf(g,'DPB0')       %set trace B OFF
    info.display=0;         %set as single plot
    info.numdata = 1;
    data{1}(:,2)=str2num(query(g,'A?'));
    info.unit = input('What is the unit of the spectrum? ','s');
    keyboard
else
    fprintf(g,'DPB1')       %set trace B ON
    info.display=1;         %set as dual plot
    info.numdata = 2;
    data{2}=data{1};
    data{1}(:,2)=str2num(query(g,'A?'));
    data{2}(:,2)=str2num(query(g,'B?'));
    info.unit.data1= deblank(query(g,'UNITA?'));
    info.unit.data2='deg';
end
```

Figure 18: HP4195 Network Analyzer Data Acquisition driver function to be used with getgpib-data.m written by Jameson Rollins.